Kinetics of H_2 passivation of Si nanocrystals in SiO_2

A. R. Wilkinson and R. G. Elliman
Department of Electronic Materials Engineering, Research School of Physical Sciences and Engineering, The Australian National University, Canberra, ACT, 0200, Australia

(Received 14 April 2003; revised manuscript received 11 June 2003; published 2 October 2003)

Time-resolved photoluminescence measurements were used to study the passivation kinetics of luminescence-quenching defects, associated with Si nanocrystals in SiO_2, during isothermal and isochronal annealing in molecular hydrogen. The passivation of these defects was modeled using the generalized simple thermal model of simultaneous passivation and dissociation, proposed by Stesmans. Values for the reaction-rate parameters were determined and found to be in excellent agreement with values previously determined for paramagnetic Si dangling-bond defects (P_b-type centers) found at planar Si/SiO_2 interfaces; supporting the view that nonradiative recombination in Si nanocrystals is dominated by such defects.

DOI: 10.1103/PhysRevB.68.155302 PACS number(s): 81.07.Bc, 73.63.Bd, 78.67.Bf

I. INTRODUCTION

Thermal oxidation of Si creates interfacial defects as a result of strain. These can act as charge traps and thereby adversely affect the operation of metal-oxide-semiconductor (MOS) devices. The minimization of such defects is a critical step in the fabrication of these devices, and it has long been known that hydrogen participates in the passivation of electrically active defects.[1] In particular, P_b-type defects ($\cdot Si \equiv Si_3$), which are known to be a major source of charge trapping at the Si/SiO_2 interface, can be electrically inactivated through chemical reaction with hydrogen.[2] Consequently, a post-metallization anneal (PMA) in forming gas (10–30% H_2 in N_2) has become standard practice in device manufacturing.[1] Early work by Brower[3,4] and more recent studies by Stesmans[5–8] have brought insight to the underlying kinetics of this process for planar interfaces.

Si nanocrystals embedded in SiO_2 exhibit strong room-temperature luminescence as a direct consequence of their small size.[9–13] As such, they offer the potential to combine electronic and optical functionality in Si-based devices. They are generally fabricated by the precipitation of excess Si in silicon-rich oxides (SRO), where the latter are produced either during deposition, using techniques such as plasma-enhanced chemical vapor deposition (PECVD), or subsequent to the growth of a stoichiometric SiO_2 layer by ion implantation of Si. Precipitation typically requires temperatures in the range of 1000–1100 °C and produces nanocrystals with mean diameters in the range of 3–5 nm.[13] Importantly, the SiO_2 acts to passivate the surface of the Si nanocrystals; reducing the number of surface defects and enhancing the luminescence efficiency. Si nanocrystals prepared in this way are approximately spherical in shape and likely have a range of crystallographic surface orientations (larger nanocrystals might be expected to have {111} facets, as these are the minimum energy surfaces). Despite the different geometry, the same interface defects prevalent in Si-based MOS devices are thought also to occur at the Si nanocrystal/oxide interface.[14–16]

It has been shown that one dangling bond defect is enough to quench the visible luminescence of a Si nanocrystal.[17] Consequently, hydrogen passivation of nanocrystals has been shown to considerably increase their luminescence efficiency by inactivating these defects.[18–24] Passivation is usually achieved by thermal annealing of the nanocrystals in forming gas, although ion implantation of hydrogen or deuterium with subsequent thermal treatment can be used to similar effect.[19] Despite the importance of the passivation process in achieving maximum luminescence, the kinetics of this process has not yet been fully explored.

II. KINETICS OF PASSIVATION AND DISSOCIATION

Interfacial dangling bonds, of which the P_b defects are an important class, result from the lattice mismatch between Si and SiO_2.[5] They have been studied in detail by electron-spin resonance (ESR) and electrical methods,[25] though ESR is typically used to detect these paramagnetic defects. At the (111) Si/SiO_2 interface, only one type of defect is observed by ESR, known as the P_b center, whereas the technologically dominant (100) Si/SiO_2 contains P_{b0} and P_{b1} variants.[6] The P_{b0} defect is always encountered, whereas the appearance of the P_{b1} defect appears to require a minimum level of thermal interfacial relaxation.[26] Studies suggest that the P_b and P_{b0} variants are chemically identical and both have been identified as electrical interface traps.[5]

From early work by Brower[3,4] on open (111) Si/SiO_2 structures, the thermal passivation of P_b defects in molecular H_2 and dissociation in vacuum are modeled by basic chemical reactions in which the reaction is limited by the availability of ''reactive'' sites,

$$P_b + H_2 \xrightarrow{k_f} P_b H + H \quad \text{for passivation, and} \tag{1}$$

$$P_b H \xrightarrow{k_d} P_b + H \quad \text{for dissociation,} \tag{2}$$

where the forward and dissociation rate constants are given by the Arrhenius expressions $k_f = k_{f0} \exp(-E_f/kT)$ and $k_d = k_{d0} \exp(-E_d/kT)$, respectively. This model relies on the high-diffusivity of molecular H_2 in SiO_2, implying that the passivation process is reaction limited, not diffusion limited.

Using square brackets to denote concentration, the rate equations for passivation and depassivation are then respectively given by

$$\frac{d[P_b]}{dt} = -k_f[H_2][P_b], \tag{3}$$

and

$$\frac{d[P_b]}{dt} = k_d[P_bH] = k_d(N_0 - [P_b]), \tag{4}$$

which, for independent reactions, lead to the simple exponential decay solutions

$$\frac{[P_b]}{N_0} = \exp(-k_f[H_2]t), \tag{5}$$

and

$$\frac{[P_b]}{N_0} = 1 - \exp(-k_d t), \tag{6}$$

where $N_0 = [P_b] + [P_bH]$, the maximum number of defects. $[H_2]$ is the volume concentration of H_2 at the Si/SiO_2 interfaces, E_f and E_d are the respective activation energies for passivation and dissociation, and k is Boltzmann's constant.

Later work by Stesmans revealed the existence of distinct spreads, σ_{Ef} and σ_{Ed}, in the activation energies E_f and E_d, respectively. The spreads are seen as a natural result of site-to-site variations in the P_b defect morphology induced by nonuniform interfacial stress, the resulting strain affecting the individual P_b—H bond strengths via weak orbital rearrangements of the unpaired Si sp^3 hybrids.[5] The magnitudes of the spreads are not unique as they depend on the thermal history of the SiO_2 structure.[5]

Including the spreads in Brower's model, a generalized consistent simple thermal (GST) model was attained by Stesmans,[6] which accurately described the kinetics of passivation and dissociation, accounting for all experimental data. By convoluting a Gaussian spread in activation energies with Brower's equations, Stesmans obtained

$$\frac{[P_b]}{N_0} = \frac{1}{\sqrt{2\pi}\sigma_{E_f}} \int_0^\infty \exp - \left[\frac{(E_{fi} - E_f)^2}{2\sigma_{E_f}^2} + tk_{f0}[H_2]\exp(-E_{fi}/kT) \right] dE_{fi}, \tag{7}$$

and

$$\frac{[P_b]}{N_0} = 1 - \frac{1}{\sqrt{2\pi}\sigma_{E_d}} \int_0^\infty \exp - \left[\frac{(E_{di} - E_d)^2}{2\sigma_{E_d}^2} + tk_{d0}\exp(-E_{di}/kT) \right] dE_{di}, \tag{8}$$

where $k_d = k_{d0}\exp(-E_{di}/kT)$ and $k_f = k_{f0}\exp(-E_{fj}/kT)$. E_f and E_d now represent mean activation energies.

In general, both reactions will proceed concurrently, so that during passivation in H_2 the reverse reaction (dissociation) will occur if the temperature is high enough. As outlined by Stesmans,[6] by coupling Brower's equations [Eqs. (3) and (4)] under the condition that $[H_2]$ at the interface is in continual equilibrium with the ambient $[H_2]$, the full interaction case for passivation in H_2 (starting from an exhaustively dissociated P_b system) is given by

$$\frac{[P_b]}{N_0} = \frac{1}{2\pi\sigma_{E_f}\sigma_{E_d}} \int_0^\infty \int_0^\infty \exp\left[- \frac{(E_{di} - E_d)^2}{2\sigma_{E_d}^2} - \frac{(E_{fj} - E_f)^2}{2\sigma_{E_f}^2} \right] \times \frac{1}{k_d + k_f[H_2]} \{k_d + k_f[H_2]\exp[-(k_d + k_f[H_2])t]\} \times dE_{di}dE_{fj}, \tag{9}$$

where a Gaussian spread in activation in both the forward and dissociation energies has been incorporated. The integration ranges can be reduced so they only include possible E_{di} and E_{fj} values.

The hydrogen concentration in the sample is calculated assuming that the H_2 diffuses very rapidly through the oxide, as shown by Shelby.[27] $[H_2]$ corresponds to the physical solubility of H_2 in vitreous silica so the amount of H_2 in solution at low pressures (P) is given by

$$[H_2] = C_0 = K(T)PV^{-1}, \tag{10}$$

where V^{-1} is the concentration of sites into which H_2 dissolves in vitreous silica (1.27×10^{21} sites/cm^3),[27] and $K(T)$ is specified by the expression[28]

$$K(T) = \left[\frac{h^2}{2\pi mkT} \right]^{3/2} \left[\frac{1}{kT} \right] \left[\frac{\exp(-h\nu/2kT)}{1 - \exp(-h\nu/kT)} \right]^3 \exp(-\varepsilon/kT). \tag{11}$$

The attempt frequency ν corresponds to 4.1×10^{12} Hz for H_2 in vitreous SiO_2. The binding energy ε for a molecule of hydrogen of mass m to a SiO_2 surface site is -0.105 eV, and corresponds to the heat of adsorption at the surface.[27] The values for vitreous SiO_2 are assumed to be equivalent to those of thermally grown SiO_2.

III. RELATING NANOCRYSTAL LUMINESCENCE TO DEFECT DENSITY

Time-resolved photoluminescence (PL) can be used to extract the rise and decay lifetimes of the nanocrystal luminescence by modulating the excitation source. The luminescence decay is characterized by a stretched exponential shape,[29,30] given by

$$I(t) = I_0 \exp\left[-\left(\frac{t}{\tau} \right)^\beta \right], \tag{12}$$

where $I(t)$ and I_0 are the intensity as a function of time and at $t = 0$, respectively. τ and β are both wavelength dependent and are respectively the lifetime and a dispersion factor whose value is a measure of the interaction strength among

Si nanocrystals. In practice, usually $\beta<1$ since $\beta=1$ yields a simple exponential and corresponds to completely isolated nanocrystals (no interaction).

Once the excitation source is turned on, the luminescence rise time τ_{on} can be expressed as $\tau_{on}^{-1}=\sigma\phi+\tau^{-1}$.[31] Thus if $\sigma\phi\ll\tau^{-1}$, then $\tau_{on}\approx\tau$ and we are in the low pump power regime, where σ is the nanocrystal excitation cross section and ϕ is the photon flux. In this regime, the PL intensity of the emitting centers can be approximated by the following expression[32]

$$I=\sigma\phi\frac{\tau}{\tau_R}n^*, \tag{13}$$

where τ_R is the radiative lifetime and n^* is the total number of Si nanocrystals that are able to emit. Equation (13) shows that, for constant excitation conditions, a variation of the luminescence yield can only be due to a change in τ or n^* or both, since τ_R and σ are independent of defect effects. This allows the extraction of n^*, the number of emitting nanocrystals, from the PL intensity and lifetime.

A quick check of the experimental parameters employed in this study confirms the validity of the low pump approximation. [For Si nanocrystals with diameters in the range of 3–5 nm, σ has a value of $\approx 1\times10^{-16}$ cm^2.[31] The photon flux $\phi\approx 2.5\times10^{18}$ cm^{-2} s^{-1} (for a 10-mW laser at 488 nm with a spot size of 1 mm^2) giving $\sigma\phi\approx 2.5\times10^2$. $\tau^{-1}>1\times10^4$ was measured for all samples. This was also directly verified by measuring the rise and decay lifetimes experimentally.]

It has been shown that a nanocrystal effectively becomes ''dark'' (stops luminescing) when it contains at least one defect. This is because in the visible PL range the nonradiative capture by neutral dangling bonds is much faster than radiative recombination.[17] Consequently, assuming a linear relationship between the number of defects and defective nanocrystals,

$$[P_b]\propto n_{dark}=n_{total}-n^*, \tag{14}$$

and

$$N_0\propto n_{total}-n^*_{ref}, \tag{15}$$

where n_{total} is the total number of nanocrystals (a constant) and n_{dark} are the nanocrystals that contain at least one defect and therefore do not luminesce. n^*_{ref} is constant as it is the number of luminescing nanocrystals in the reference sample, which contains the maximum number of recoverable defects N_0. The reference sample is the unpassivated sample, so $[P_b]/N_0\leqslant 1$. The proportionality constants for Eqs. (14) and (15) will be the same, so using these equations we can write

$$\frac{N_0-[P_b]}{N_0}\propto n^*-n^*_{ref}, \tag{16}$$

and so

$$n^*-n^*_{ref}\propto 1-\frac{[P_b]}{N_0}. \tag{17}$$

It is convenient to express the number of emitting nanocrystals relative to the reference sample, from Eq. (13),

$$\frac{n^*}{n^*_{ref}}=\frac{I}{I_{ref}}\frac{\tau_{ref}}{\tau}, \tag{18}$$

since $\sigma\phi$ is kept constant and τ_R is independent of defect effects.

We now have a procedure to relate the luminescence intensity and lifetime to the relative defect density. This allows one to apply Stesmans' GST model to extract the chemical kinetics of the hydrogen passivation process of Si nanocrystals in SiO_2, through time-resolved PL measurements. It should be stated that whereas ESR specifically probes for paramagnetic P_b defects, the PL measurements are not defect specific. Therefore the reaction-rate parameters extracted by this technique are mean values corresponding to all the luminescence-quenching defects that can be passivated by hydrogen. This said, the quenching of nanocrystals luminescence is thought to be dominated by defects at the interface, where P_b defects are found.

IV. EXPERIMENTAL DETAILS

A. Sample preparation

Si nanocrystals were synthesized by ion implantation of Si^+ into 1.25-μm SiO_2 layers grown by wet thermal oxidation at 1100 °C on B-doped (0.1–0.3 Ω cm) Czochralski (100) Si. The samples were implanted at an energy of 400 keV to a fluence of 2×10^{17} cm^{-2}, at room temperature. This results in a Si concentration profile with a peak excess of close to 10 at.% at a projected range of 630 nm and a straggle of 140 nm, calculated using TRIM.[33] The as-implanted samples, placed in a quartz boat, were annealed at 1100 °C in high-purity Ar (99.997%) for 1 h in a conventional quartz-tube furnace. This is a standard thermal treatment used to produce luminescent nanocrystals, with the high-temperature required to remove implantation damage (such as nonbridging oxygen-hole centers and oxygen vacancies)[34] and precipitate the crystals. The sample at this stage contains the maximum number of recoverable defects and was used as the reference sample. After one hour, a large number of P_b-type defects are created as the nanocrystals precipitate, with longer annealing times reducing their density.[16]

Hydrogen passivation anneals were performed in high-purity (99.98%) forming gas (5% H_2 in N_2). Samples were annealed either isochronally or isothermally. Isochronal anneals were performed for 1 h in the temperature range of 100–800 °C. Isothermal anneals were performed at four set temperatures (nominally 300, 350, 400, and 500 °C) for times ranging from 1 min to 16 h. A rapid thermal processor (AET Thermal RX) was used for annealing times $\leqslant$10 min, with the conventional tube furnace used for all longer anneals. At the completion of each anneal, the sample was withdrawn to the cool zone of the furnace and cooled to room temperature in the forming gas ambient.

Hydrogen dissociation was performed in a N_2 ambient (99.99%) on samples previously annealed in forming gas at

TABLE I. Kinetic parameters for thermal passivation in H_2 (this work in 5% H_2 in N_2) and dissociation in vacuum (this work in N_2) of P_b-type defects at the Si/SiO_2 interface.

		E_f (eV)	σ_{Ef} (eV)	k_{f0} (10^{-8} cm^3 s^{-1})	E_d (eV)	σ_{Ed} (eV)	k_{d0} (10^{13} s^{-1})
This work	P_b type	1.68 ± 0.04	0.18 ± 0.02	9 ± 5	2.9 ± 0.05	0.29 ± 0.03	2 ± 1
(111)	P_b:	1.51 ± 0.04[a]	0.060 ± 0.004[a]	$9.8(+8/-5)$[a]	2.83 ± 0.03[a]	0.09 ± 0.03[a]	1.6 ± 0.5[a]
Si/SiO_2							
(100)	P_{b0}:	1.51 ± 0.03[b]	0.14 ± 0.02[b]	143 ± 60[b]	2.86 ± 0.04[c]	0.17[c,d]	2[c,e]
Si/SiO_2	P_{b1}:	1.57 ± 0.03[b]	0.15 ± 0.03[b]	143 ± 60[b]	2.91 ± 0.03[c]		2[c,e]

[a]Reference 6.
[b]Reference 8.
[c]Reference 35.
[d]Stathis suggested an overall σ_{Ed} value of 0.17 eV for P_{b0} and P_{b1} combined.
[e]This parameter (k_{d0}) was fixed at a value of 2×10^{13} s^{-1} based on physical insight (frequency of the Si-H wagging mode).

500 °C for 1 h. The initial passivation treatment establishes the starting condition for the dissociation study. 1-h isochronal anneals were performed at temperatures in the range of 200–800 °C.

It should be noted that the conditions used in this work for hydrogen passivation and dissociation are similar, but not identical, to those used by other authors. For the values shown in Table I, hydrogen passivation was carried out in 1.1 atm H_2 (99.9999%) and dissociation was performed in vacuum. Nonetheless, the partial pressure of H_2 is taken into account in the modeling.

B. PL and time-resolved PL

Photoluminescence (PL) measurements were performed at room temperature, using the 488-nm line of an Ar^+ ion laser as the excitation source. Emitted light was analyzed using a single grating monochromator (TRIAX-320) and detected with a liquid-nitrogen-cooled front-illuminated open-electrode charge-coupled device (CCD) array (EEV CCD30-11).

Time-resolved PL measurements were performed by modulating the laser beam with an acousto-optic modulator (Brimrose TEM-85-10). A room-temperature photomultiplier (Hamamatsu R928) was used to detect the light from the exit port of the monochromator with the grating centered at 800 nm (bandpass of 40 nm). The signal from the photomultiplier was collected using a digital storage oscilloscope. Emission decay lifetimes were extracted by the least-squares fitting of a stretched exponential [Eq. (12)]. The timing resolution of the system is $<1\ \mu$s.

V. EXPERIMENTAL RESULTS

Figure 1 shows the effect of H passivation on the nanocrystal PL, at a range of annealing temperatures in forming gas. The increase in PL intensity is due to the passivation of nonradiative defects at the nanocrystal/oxide interface. The shaded region represents the approximate detection window used in time-resolved PL measurements (equal to the bandpass of the monochromator centered at 800 nm). The choice of this window is arbitrary, as the trend of increasing intensity with improved passivation was found to be comparable across the whole PL spectrum.

Figure 2 shows a semilogarithmic plot of the luminescence decay-time measurements for the reference sample before and after passivation at 500 °C for 1 h in forming gas. The decay curves are clearly nonlinear, and thus not well described by a simple exponential. As expected, they are well characterized by a stretched exponential shape. Fitting the PL decay curves with Eq. (12) allows the extraction of τ and β as a function of the passivation and desorption anneal schedule. These values are shown in Figs. 3 and 4, respectively.

The measured luminescence decay lifetime can be approximated by $\tau^{-1}=\tau_R^{-1}+\tau_{NR}^{-1}$, where τ_R is the nanocrystal radiative lifetime and τ_{NR} is the nonradiative lifetime (associated with defects and/or exciton energy migration). Consequently, as defects, which act as fast nonradiative recombination states, are passivated (eliminated), τ_{NR} increases and τ

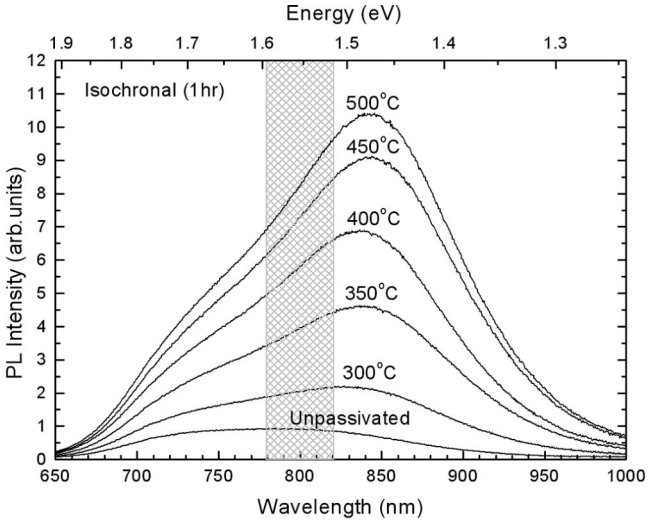

FIG. 1. Typical nanocrystal PL spectra of the reference sample (unpassivated) after annealing for 1 h in 5% H_2 in N_2 at different temperatures. The annealing temperatures are indicated in the figure. The shaded box indicates the approximate detection window used for time-resolved PL measurements.

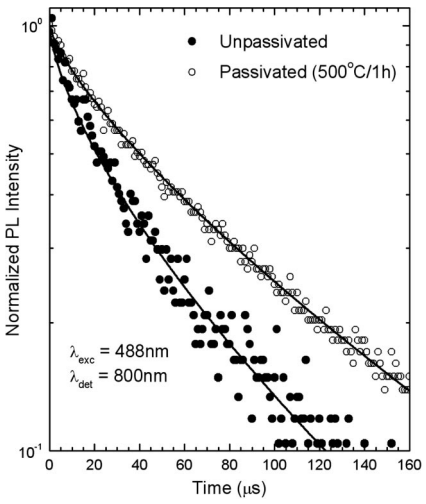

FIG. 2. Typical normalized decay-time measurements of the PL signal at 800 nm for the reference sample before and after annealing in forming gas at 500 °C for 1 h. The solid lines are stretched exponential fits [Eq. (12)]. Data were taken at room temperature.

approaches τ_R. The nanocrystals also become more isolated due to the concomitant reduction in exciton migration channels. The complete model of this process is unclear, as the source and mechanism of luminescence from Si nanocrystals is still under debate. However, a reduction of fast-recombination sites, whether defects at the interface or within the oxide, is consistent with the observed increase in τ and β as the extent of passivation increases.

The fitting of Eq. (12) also enables the extraction of the intensity and lifetime enhancement for each sample, I/I_{ref} and τ/τ_{ref} respectively, due to hydrogen passivation. These quantities, along with Eq. (18), then allow the corresponding enhancement of emitting nanocrystals to be determined. The results for the isochronal absorption and dissociation studies

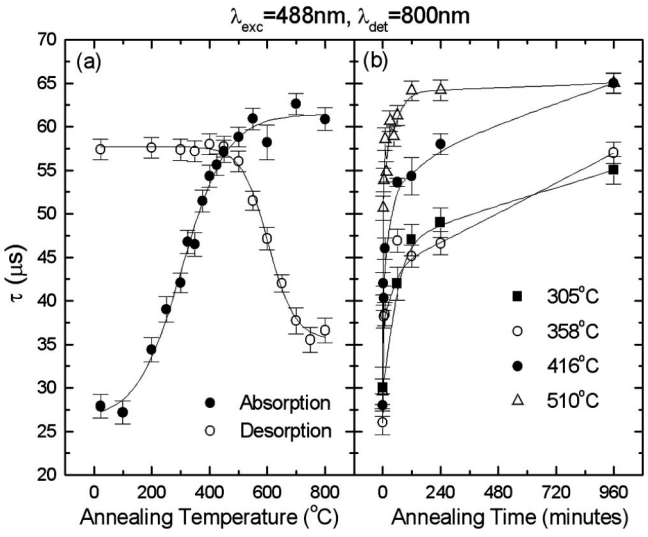

FIG. 3. Plots of the luminescence decay lifetime for (a) the isochronal ($t=1$ h) study, and (b) the isothermal study. Data are extracted from time-resolved PL measurements fitted with Eq. (12). The solid lines are provided as a guide to the eye only.

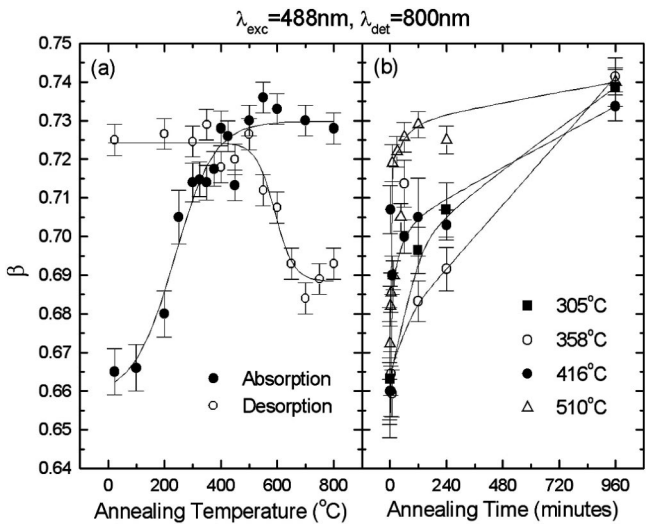

FIG. 4. Plots of the dispersion factor for (a) the isochronal study, and (b) the isothermal study. Data are extracted from time-resolved PL measurements fitted with Eq. (12). The solid lines are provided as a guide to the eye only.

are shown in Fig. 5, and the isothermal absorption study in Fig. 6.

In Fig. 5, a factor of ≈ 6 increase is seen in intensity with optimum passivation, which is accounted for by a doubling

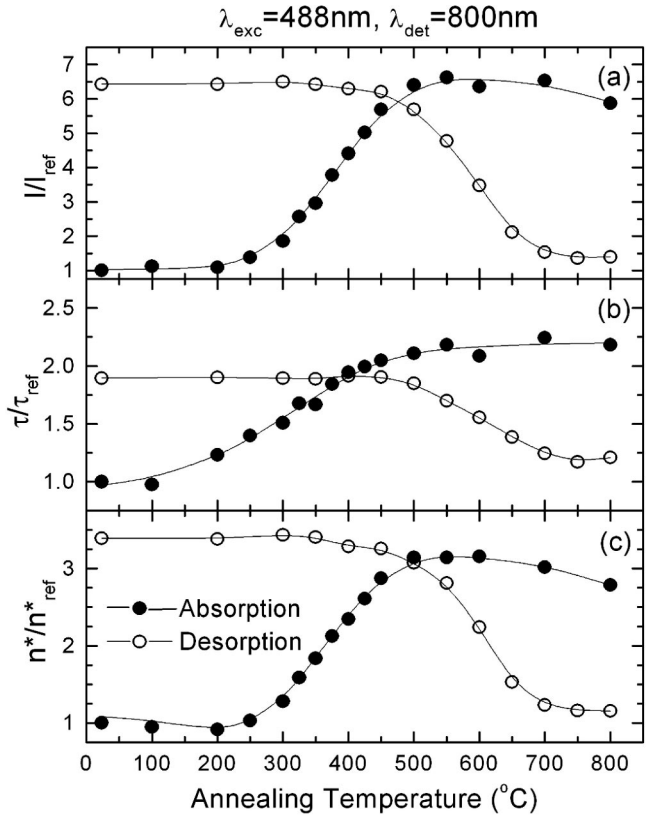

FIG. 5. Plots of relative (a) intensity, (b) lifetime, and (c) emitting nanocrystals [from Eq. (18)] versus annealing temperature, during H passivation for 1 h in 5% H_2. Data are from time-resolved PL measurements. The lines are provided as a guide to the eye only.

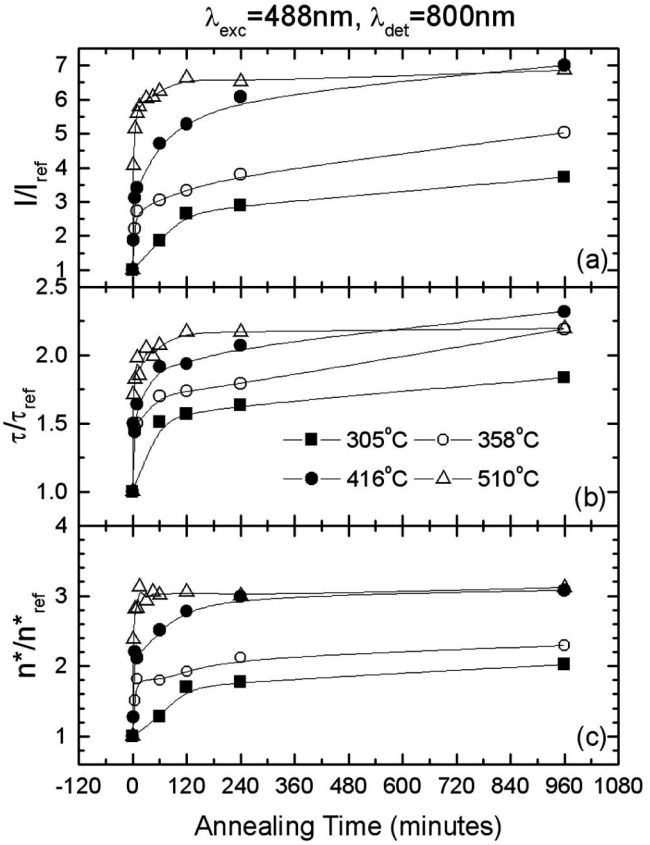

FIG. 6. Plots of relative (a) intensity, (b) lifetime, and (c) emitting nanocrystals [from Eq. (18)] versus annealing time, during H passivation at 500 °C in 5% H_2. Data are extracted from time-resolved PL measurements. The lines are provided as a guide to the eye only.

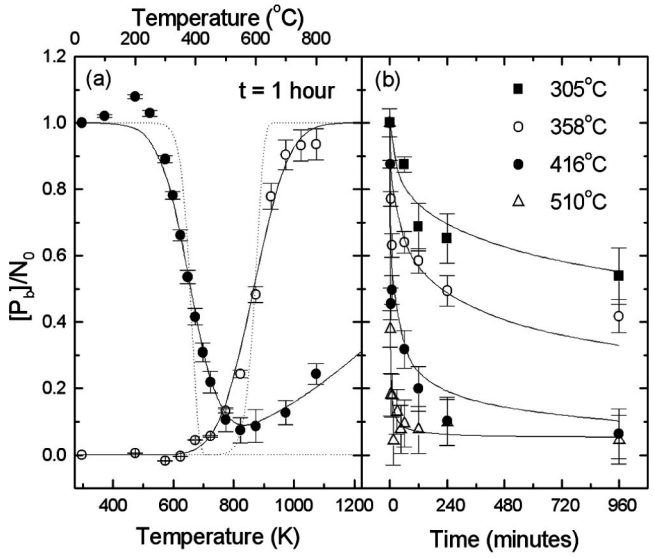

FIG. 7. Plots relative P_b defect concentration versus (a) annealing temperature of hydrogen passivation (solid circles) and dissociation (open circles) and (b) annealing time, during hydrogen passivation at 305, 358, 416, and 510 °C. The solid lines represent the global least-squares fit of the GST model [Eq. (8) (for dissociation only) and Eq. (9)] to experimental data derived from time-resolved PL measurements through Eqs. (17) and (18). The dotted lines are Brower's simple thermal model for passivation and dissociation [Eqs. (5) and (6)].

of lifetime and a tripling of the number of luminescing nanocrystals [using Eq. (18)]. The action of simultaneous desorption limits the level of maximum passivation, as hydrogen is dissociated from the defects above about 450 °C. The hydrogen desorption study also shows that at high temperatures, where all hydrogen should be lost from the sample, the luminescence intensity and lifetime do not return completely to their pre-passivation values. This is thought to be due to a partial relaxation of interfacial strain present in the samples after the nanocrystals are formed at 1100 °C. This strain is due to the difference in thermal coefficient of expansion between Si and SiO_2, which causes strain as the samples are cooled. This effect is independent of the presence of hydrogen as it has been seen in samples where no hydrogen is present.

In Fig. 6, the isothermal data show the same trend of increasing intensity and lifetime with improved passivation as was seen in the isochronal case (Fig. 5). As expected, the samples annealed at higher temperatures approach optimum passivation more quickly. However, due to competition from the desorption reaction, samples annealed for 1 h at higher temperatures will be less well passivated than those annealed at the optimum temperature around 500 °C. Similarly, samples annealed at lower temperatures require much greater annealing time to achieve similar levels of passivation. [This is highlighted by the data in Fig. 6(c), which show that the degree of passivation achieved after 1 h at 510 °C will not be achieved at 305 °C even after several days annealing. That said, increasing $[H_2]$ in the sample through annealing in pure H_2 and/or at increased pressure would reduce this time.]

VI. MODELING THE KINETICS

A global least-squares fit (of all data shown in Fig. 7) was used to determine the parameters shown in Table I, for this work. For convenience, the values obtained by others for molecular hydrogen passivation and dissociation of paramagnetic P_b defects for planar (111) and (100) Si/SiO_2 interfaces are also included. A global fit of data over a large range is important to give uniqueness to the fit. For example, a fit of isochronal data alone can be described equally well by a range of parameter sets. The full-interaction GST model [Eq. (9)] was used to model the passivation kinetics (simultaneous passivation and dissociation), whereas the simpler case of pure desorption was modeled using Eq. (8). The proportionality constant [for Eq. (17)] between experimental data and the model was also left as a fitting parameter. A partial pressure of 0.05 atm was used in Eq. (10) in determining $[H_2]$, due to the forming gas used for passivation having a concentration of 5% hydrogen.

The values obtained in this work are in general agreement with those measured for (100) and (111) planar interfaces. This supports the view that similar defects and processes are involved in both cases. It can be noted, however, that the activation energy for the passivation reaction and the spread of activation energies for the desorption reaction both appear

slightly higher than the values determined for planar interfaces. There are several possible reasons for this variation, the most obvious being: (a) the difference in interface geometry because of the approximately spherical shape of the nanocrystals; and (b) differences in the range of luminescence-killing defects involved. For example, Gheorghita *et al.*[36] identified the *R* defect at the (111) Si/SiO_2 interface, which was also found to be passivated by H_2 albeit with a very different activation energy and rate constant. However, Stesmans found for (111) Si/SiO_2 that $\sigma_{Ef}/E_f \approx \sigma_{Ed}/E_d$ and $\sigma_{Ef}/\sigma_{Ed}=1.5$.[5] This is similar to that found in this work, with $\sigma_{Ef}/E_f \approx \sigma_{Ed}/E_d \approx 10\%$ and $\sigma_{Ef}/\sigma_{Ed}=1.6$. Stesmans related σ_{Ef} and σ_{Ed} to interfacial stress, which affects the spread in P_b defect morphology. This suggests that σ_{Ef} and σ_{Ed} found in this work relate to a higher mean interfacial stress than is generally found at planar interfaces.

To gain confidence in the extracted parameters, the consistency of these parameters can be compared to the underlying physical insight. A simple model from Brower[3] predicts a k_{f0} on the order of 9.7×10^{-8} $cm^3\,s^{-1}$. The value obtained in this work agrees well with this value and that obtained by Stesmans for (111) Si/SiO_2. It has been determined that the low-frequency Si-H wagging mode (Si≡Si-H), at 1.86×10^{13} s^{-1},[37] controls thermal interfacial Si-H breaking.[7] The value of $(2\pm1)\times10^{13}$ s^{-1} obtained in this work also agrees well with this value.

The net effect of Eqs. (1) and (2) is the dissociation of the H_2 molecule, with both steps resulting in emission of a hydrogen atom. Therefore the value for H_2 dissociation in vacuum (4.52 eV at 298 K) (Ref. 38) can be compared to the sum of the forward and dissociation activation energies E_f and E_d, respectively. Stesmans found for (111) Si/SiO_2 a net apparent activation energy of 4.34 ± 0.06 eV and slightly higher for (100) Si/SiO_2. In this work, a net apparent activation energy of 4.58 ± 0.07 eV was found, which agrees well with the value for dissociation in vacuum.

VII. CONCLUDING REMARKS

Using time-resolved PL, the hydrogen passivation kinetics of Si nanocrystals embedded in SiO_2 has been studied both isothermally and isochronally, providing a sufficient set of data to extract the reaction-rate parameters with some confidence. The GST model proposed by Stesmans was found to well describe the passivation process of Si nanocrystals in SiO_2. The reaction-rate parameters were found to be $E_f=1.68$ eV, $\sigma_{Ef}=0.18$ eV, $k_{f0}=9\times10^{-8}$ $cm^3\,s^{-1}$ for hydrogen passivation and $E_d=2.9$ eV, $\sigma_{Ed}=0.29$ eV, $k_{d0}=2\times10^{13}$ s^{-1} for hydrogen dissociation. The similarity of these values to those found for P_b defects at planar Si/SiO_2 interfaces supports the view that nonradiative recombination is dominated by such defects. The modeling has also highlighted that the simultaneous desorption limits the level of passivation attainable. If the passivation temperature is too high, the desorption reaction dominates. This means that a one-step anneal to both precipitate and passivate the nanocrystals at 1100 °C in forming gas will not achieve the same quality of passivation as a two-step anneal (at 1100 °C) and passivation (at 500 °C) sequence. Moreover, for high-temperature annealing the final level of passivation will depend on the cooling rate. On the other hand, using low passivation temperatures to avoid desorption will require extended annealing times. Finally, this work has shown that nanocrystals provide a useful model system for studying such processes using PL. However, since PL is unable to unambiguously identify specific defects, it cannot replace, but instead complements, the more complex ESR.

[1] Y. C. Cheng, Prog. Surf. Sci. **8**, 181 (1977).
[2] E. H. Poindexter and P. J. Caplan, Prog. Surf. Sci. **14**, 201 (1983).
[3] K. L. Brower, Phys. Rev. B **38**, 9657 (1988).
[4] K. L. Brower, Phys. Rev. B **42**, 3444 (1990).
[5] A. Stesmans, J. Appl. Phys. **92**, 1317 (2002).
[6] A. Stesmans, J. Appl. Phys. **88**, 489 (2000).
[7] A. Stesmans, Phys. Rev. B **61**, 8393 (2000).
[8] A. Stesmans, Solid State Commun. **97**, 255 (1996).
[9] T. Shimizu-Iwayama, N. Kurumado, D. E. Hole, and P. D. Townsend, J. Appl. Phys. **83**, 6018 (1998).
[10] D. Kovalev, H. Heckler, G. Polisski, and F. Koch, Phys. Status Solidi B **215**, 871 (1999).
[11] M. L. Brongersma, A. Polman, K. S. Min, and H. A. Atwater, J. Appl. Phys. **86**, 759 (1999).
[12] F. Iacona, G. Franzò, and C. Spinella, J. Appl. Phys. **87**, 1295 (2000).
[13] B. G. Fernandez, M. López, C. García, A. Pérez-Rodríguez, J. R. Morante, C. Bonafos, M. Carrada, and A. Claverie, J. Appl. Phys. **91**, 798 (2002).
[14] M. S. Brandt and M. Stutzmann, Appl. Phys. Lett. **61**, 2569 (1992).
[15] H. J. v. Bardeleben, M. Chamarro, A. Grosman, V. Morazzani, C. Ortega, J. Siejka, and S. Rigo, J. Lumin. **57**, 39 (1993).
[16] M. López, B. Garrido, C. García, P. Pellegrino, A. Pérez-Rodríguez, J. Morante, C. Bonafos, M. Carrada, and A. Claverie, Appl. Phys. Lett. **80**, 1637 (2002).
[17] M. Lannoo, C. Delerue, and G. Allan, J. Lumin. **70**, 170 (1996).
[18] E. Neufield, S. Wang, R. Apetz, C. Buchal, R. Carius, C. W. White, and D. K. Thomas, Thin Solid Films **294**, 238 (1997).
[19] K. S. Min, K. V. Shcheglov, C. M. Yang, H. A. Atwater, M. L. Brongersma, and A. Polman, Appl. Phys. Lett. **69**, 2033 (1996).
[20] S. Cheylan and R. G. Elliman, Nucl. Instrum. Methods Phys. Res. B **148**, 986 (1999).
[21] S. P. Withrow, C. W. White, A. Meldrum, J. D. Budai, D. M. Hembree, Jr., and J. C. Barbour, J. Appl. Phys. **86**, 396 (1999).
[22] S. Cheylan and R. G. Elliman, Appl. Phys. Lett. **78**, 1225 (2001).
[23] S. Cheylan and R. G. Elliman, Appl. Phys. Lett. **78**, 1912 (2001).
[24] S. Cheylan and R. G. Elliman, Nucl. Instrum. Methods Phys. Res. B **175–177**, 422 (2001).
[25] E. H. Poindexter, Semicond. Sci. Technol. **4**, 961 (1989).
[26] A. Stesmans and V. V. Afanas'ev, Appl. Phys. Lett. **77**, 1469 (2000).

[27] J. E. Shelby, J. Appl. Phys. **48**, 3387 (1977).
[28] J. F. Shackelford, P. L. Studt, and R. M. Fulrath, J. Appl. Phys. **43**, 1619 (1972).
[29] J. Linnros, A. Galeckas, N. Lalic, and V. Grivickas, Thin Solid Films **297**, 167 (1997).
[30] L. Pavesi and M. Cescini, Phys. Rev. B **48**, 17 625 (1993).
[31] F. Priolo, G. Franzò, D. Pacifici, V. Vinciguerra, F. Iacona, and A. Irrera, J. Appl. Phys. **89**, 264 (2001).
[32] D. Pacifici, E. C. Moreira, G. Franzò, V. Martorino, and F. Priolo, Phys. Rev. B **65**, 144109 (2002).
[33] J. F. Ziegler, J. P. Biersack, and U. Littmark, *The Stopping and Range of Ions in Solids* (Pergamon, New York, 1985).
[34] M. Y. Valahk, V. A. Yukhimchuk, V. Y. Bratus', A. A. Konchits, P. L. F. Hemment, and T. Komoda, J. Appl. Phys. **85**, 168 (1999).
[35] J. H. Stathis, J. Appl. Phys. **77**, 6205 (1995).
[36] L. Gheorghita and E. Ogryzlo, J. Appl. Phys. **87**, 7999 (2000).
[37] B. B. Stefanos, A. B. Gurevich, M. K. Weldon, K. Raghavachari, and Y. J. Chabal, Phys. Rev. Lett. **81**, 3908 (1998).
[38] J. A. Kerr, in *CRC Handbook of Chemistry and Physics*, 73rd ed., edited by D. R. Lide (CRC, Boca Raton, 1992), pp. 9–131.